Journal of Non-Newtonian Fluid Mechanics 201 (2013) 56–68

Contents lists available at ScienceDirect

Journal of Non-Newtonian Fluid Mechanics

journal homepage: http://www.elsevier.com/locate/jnnfm

Coupling of full two-dimensional and depth-averaged models for granular flows

Birte Domnik [a,*], Shiva P. Pudasaini [a], Rolf Katzenbach [b], Stephen A. Miller [a]

[a] University of Bonn, Steinmann Institute, Department of Geodynamics and Geophysics, Meckenheimer Allee 176, 53115 Bonn, Germany
[b] Darmstadt University of Technology, Institute and Laboratory of Geotechnics, Petersenstraße 13, 64287 Darmstadt, Germany

ARTICLE INFO

Article history:
Received 13 December 2012
Received in revised form 25 July 2013
Accepted 25 July 2013
Available online 1 August 2013

Keywords:
Rapid granular flows
Deposition process
Multiscale coupling strategy
Drucker–Prager yield criterion
Slip velocity
Depth-averaged granular avalanche model

ABSTRACT

We develop a full two-dimensional Coulomb-viscoplastic model and apply it for inclined channel flows of granular materials from initiation to deposition. The presented model includes the basic features and observed phenomena in dense granular flows like the exhibition of a yield strength and a non-zero slip velocity. A pressure-dependent yield strength is proposed to account for the frictional nature of granular materials. The yield strength can be related to the internal friction angle of the material and plays an important role, e.g., in deposition processes. The interaction of the flow with the solid boundary is modelled by a pressure and rate-dependent Coulomb-viscoplastic sliding law. We develop an innovative multiscale strategy to couple the full two-dimensional, non-depth-averaged model (N-DAM) with a one-dimensional, depth-averaged model (DAM). With the coupled model the computational complexity reduces dramatically by using DAM in regions with smooth changes of flow variables. In regions where depth-averaging becomes inaccurate, like in the initiation and deposition regions and particularly, when the flow hits an obstacle or a defence structure, N-DAM must be used, because in these regions the momentum transfer must be considered in all directions. The performance of the coupling is very high: The numerical results obtained by the coupled model deviate only slightly from the ones generated with the full two-dimensional model. This shows that the coupled model, which retains all the basic physics of the flow, is an attractive alternative to an expensive, full two-dimensional model.

1. Introduction

Granular flows are often encountered in geophysical contexts like debris flows, snow and rock avalanches, and also in transport processes in engineering applications [1–4]. The flow of a granular avalanche is characterised by three different flow regimes: (i) the starting zone where rupture and fragmentation of the solid material occurs and/or the granular material begins to flow, (ii) the avalanching zone where the granular material reaches fast supercritical speed, and (iii) the run-out zone where the moving mass is decelerated and comes to a rather sudden standstill [5]. Observations, both in the laboratory and nature, show flow transitions from a subcritical (Froude number < 1) to a supercritical (Froude number > 1) regime after the flow release. Further downstream, rapid flow regimes develop, which are characterised by fairly uniform velocity profiles with depth, and strong shearing in the vicinity of the base and dominant sliding at the base [2]. In the deposition regime and, in particular, in the transition region from the rapid flow into the deposition zone, shocklike structures form and an overall depth flow changes into a surface boundary layer flow, which quickly slows down and eventually settles [5,6].

Flows of dense granular materials are well described by viscoplastic constitutive laws [1,3,7–9] , in which the material yields and starts to flow once a yield criterion is satisfied. The yield criterion depends on the stress state and a yield strength, which has to be exceeded to start flowing. Bingham materials are described by a constant and empirical yield stress and flow like a viscous fluid at high stresses [10]. In applications, this simple viscoplastic rheology is often an adequate choice [11–15]. When the friction between the grains becomes considerable or even dominant, like in slow motions and especially in deposition regimes, this assumption could be too simple. Jop et al. [7] account for the frictional nature of the granular material by assuming a pressure-dependent yield stress and an effective viscosity depending on the shear rate and the local pressure. With their approach, which mainly concerns the yield criterion, the relatively slow motion of granular materials on mild inclines (close to or below the internal friction angle) is successfully described. Moriguchi et al. [9,16] proposed a Bingham type constitutive model for rapid granular flows down inclined planes hitting a rigid obstruction.

Another important aspect of granular flow simulation is the description of the interaction with the basal boundary, which is

* Corresponding author. Tel.: +49 228733058.
E-mail address: domnik@geo.uni-bonn.de (B. Domnik).

0377-0257/$ - see front matter © 2013 Elsevier B.V. All rights reserved.
http://dx.doi.org/10.1016/j.jnnfm.2013.07.005

often simplified by assuming a no-slip boundary condition [7,9,16]. However, it is observed in experiments and in the field that in rapid flow of granular material down the slopes, even the lowest particle layer in contact with the bottom boundary moves with a non-zero and non-trivial velocity [2,5,17–20]. In a viscoplastic granular flow model [15] , the Coulomb friction law is used to model the interaction of the flow with the solid basal boundary surface. The bed friction angle defines the frictional strength and depends on both the granular material and the boundary substrate. Here, we advance this model [15] by introducing a pressure-dependent yield stress, which can be related to the internal friction angle similar to Moriguchi et al. [9]. However, in contrast to Moriguchi et al. [9], we are able to describe non-zero slip velocities by the Coulomb friction law as in Domnik and Pudasaini [15]. Hence, the presented full two-dimensional Coulomb-viscoplastic granular flow model, characterised by the internal and bed friction angle, constitutes a substantial improvement of the existing models.

Depth-averaged granular flow models and simulations have been largely successful in describing flows of granular materials, avalanches and debris flows down channels and slopes [2,21–24]. Their success is basically founded on their simplicity and a typically small computational effort. Depth-averaged models are also used to describe shock-formations and flow-obstacle-interactions [6,25–32]. In these situations the validity of the assumptions made in the depth-averaged models is crucial. Although depth-averaged models are applied successfully in these situations, their success is limited to the prediction of flow depths and mean velocities. Naturally, depth-averaged models cannot predict velocity variations along the flow depth direction and also a deduction of the pressure within the material or at obstacles can only be made by deriving the pressure from the depth-averaged velocity. Full dynamical and internal pressure cannot be obtained. Therefore, those equations cannot fully and globally be applied, e.g., in situations when topography changes are large (large curvatures), in the vicinity of flow obstacle interactions, for strongly converging and diverging flows, in flow initiations, and also during deposition processes [5,6,33–36].

For a physically complete description of the flow dynamics, without reduction of the information through the flow depth, a non-depth-averaged model is required. A first step towards modelling complicated three-dimensional flows is to reduce it to two dimensions by studying an inclined chute flow [15]. Some basic two-dimensional channel flow experiments and their simulations with depth-averaged model equations are reported in Pudasaini et al. [5], dasaini and Kröner [6], Pudasaini and Domnik [37]. Nevertheless, non-depth-averaged models require very large computational costs. Therefore, it is desirable to develop a coupled hybrid model, in which the more expensive, non-depth-averaged model is solved only in some selected local domains, where depth-averaging is not appropriate, and a depth-averaged model is used in the remaining complementary domain. This coupling method represents a multiscale and multiphysics strategy, as the scale of the momentum transfer in the flow depth direction and also the applied physical model is different for the depth-averaged and non-depth-averaged subdomains. The significant advantage using the coupled model is that it requires much less computing time and provides a full two-dimensional description of the flow in the relevant regions. For instance, such a multiscale strategy is reported in Formaggia et al. [38] and Miglio et al. [39] for subcritical flows of simple Newtonian fluids. However, to our knowledge, a multiscale and multiphysics strategy has not yet been developed and applied for rapid flows of frictional granular materials on inclined channels, which are very important geophysical and industrial mass flow processes.

As the available computer power has increased enormously, discrete element methods (DEM) become more important. They compute the motion of a large number of particles and can be used to simulate a wide variety of granular flows and rock mechanics problems. Discrete particle simulations on model systems serve as a good possibility for a detailed study of the rheology of moving granular material [40–42]. Nevertheless, the number of particles that can be dealt with at the moment is limited. Therefore, their application is restricted to small scale flows [2,42]. Geophysical mass flows consist of huge volumes [4] and are thus less likely to be fully described by DEM.

In Section 2 we derive a full two-dimensional Coulomb-viscoplastic model for granular materials with a pressure-dependent yield stress. The yield stress is defined by the internal friction angle and the pressure. The interaction of the flow with the solid basal boundary surface is described by a Coulomb friction law. Section 3 is devoted to the derivation and analysis of a depth-averaged, one-dimensional granular flow model for free surface flows down an inclined channel. The constitutive behaviour of the granular material is assumed to be described by a Mohr–Coulomb yield criterion. Then in Section 4, the decomposition of the computational domain into full 2D (two-dimensional) and depth-averaged 1D (one-dimensional) regions and appropriate matching conditions at the interfaces are discussed for the coupled model. The performance of the coupled model is studied numerically in Section 5. Two different flow configurations are considered: (i) an undisturbed inclined channel flow, and (ii) a flow hitting a perpendicular wall. The correspondence between of the material parameters used in the both models (1D and 2D) is analysed. In detail, we study the impact of the interface position on the accuracy of the coupled model. Finally, some conclusions are drawn in Section 6.

2. Full 2D Coulomb-viscoplastic granular flow model

In ths section we present the full two-dimensional Coulomb-viscoplastic granular flow model, in which the pressure-dependent yield strength is introduced. The model equations and associated boundary conditions are discussed. We develop a procedure to numerically solve these equations.

2.1. Model equations

The rapid motion of a granular material in a two-dimensional inclined rectangular channel, Fig. 1, is characterised by the pressure p and the velocity $\mathbf{u} = (u, w)^T$, with u the velocity component in downslope direction (x), and w the velocity component perpendicular to the channel surface (z) . In the dense flow regime, in which variations of the (solid) volume fraction are small, granular flow can be assumed incompressible [2,7,41,43]. Nevertheless, density changes due to dilatation and compaction can become locally considerable, yet small during release, flow-obstacle interactions, or depositions. However, during long distance flows global density changes are negligible. So, in the following, granular flow is assumed incompressible and density changes are neglected. The flow in a channel inclined by an angle ζ is described by a system of partial differential equations, representing the mass and momentum balances:

$$\mathrm{div}\mathbf{u} = 0, \tag{1}$$

$$\frac{d\mathbf{u}}{dt} = \mathrm{div}\boldsymbol{\sigma} + \mathbf{g}, \tag{2}$$

where $\boldsymbol{\sigma}$ is the Cauchy stress tensor normalised by bulk density (ρ), $\mathbf{g}(\zeta) = (g\sin\zeta, -g\cos\zeta)^T$ is the gravitational acceleration with the gravity constant g, and d/dt is the material derivative.

We consider a dry dense granular material where motion and settlement are assumed to be well described by viscoplastic constitutive laws [1,3,7,8]. The normalised stress tensor (normalised by

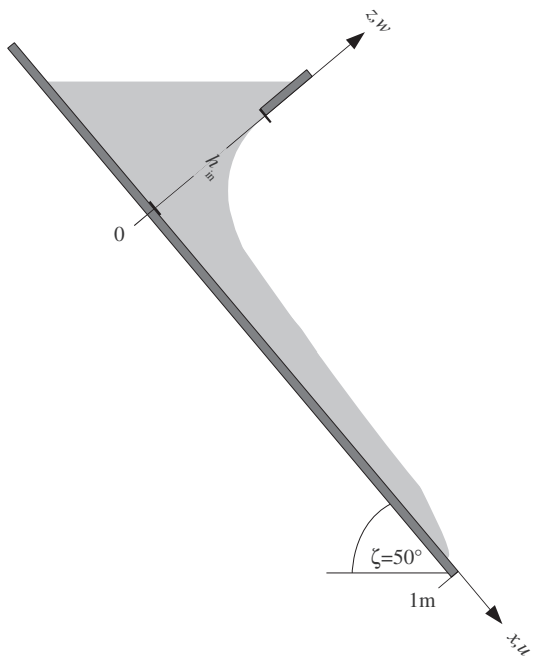

Fig. 1. Side view of an inclined chute with considered coordinate system. The x-axis is aligned in the downslope direction and the z-axis is orientated perpendicular to it. The granular material (depicted in light grey) enters the channel at $x = 0$ through a silo gate with opening height h_{in} and flows in the downslope direction. ζ is the inclination angle of the chute.

density) for a viscoplastic fluid can be described by the constitutive relation

$$\boldsymbol{\sigma} = -p\mathbb{1} + 2\nu\mathbf{D} + 2\tau_y \frac{\mathbf{D}}{\|\mathbf{D}\|}, \tag{3}$$

where p is the (normalised) pressure, the strain rate tensor is given by the symmetric part of the velocity gradient, $\mathbf{D} = 1/2[(\nabla\mathbf{u}) + (\nabla\mathbf{u})^T]$, ν represents a constant kinematic viscosity, and τ_y is the yield stress (normalised by density). The norm of the strain rate tensor is defined by $\|\mathbf{D}\| = \sqrt{2\text{tr}(\mathbf{D}^2)}$. Eq. (3) can also be written in terms of an effective viscosity

$$\nu_{\text{eff}} = \nu + \frac{\tau_y}{\|\mathbf{D}\|}, \tag{4}$$

as $\boldsymbol{\sigma} = -p\mathbb{1} + 2\nu_{\text{eff}}\mathbf{D}$. When the strain rate $\|\mathbf{D}\|$ equals zero, the effective viscosity becomes infinite. In order to avoid such infinite value, which cannot be treated in numerical simulations, usually an exponential factor is introduced

$$\nu_{\text{eff}} = \nu + \frac{\tau_y}{\|\mathbf{D}\|}\left(1 - e^{-m_y\|\mathbf{D}\|}\right). \tag{5}$$

Eq. (5) holds uniformly in yielded and unyielded regions, and the transition between these regions is smoother for smaller exponents m_y [44]. For $\tau_y = 0$ the material behaves as a Newtonian fluid. A Bingham material is described by a constant yield stress. Here, we propose a pressure-dependent yield stress to better represent the frictional nature of the granular material:

$$\tau_y = \tau_p p. \tag{6}$$

Eq. (6) forms a Drucker–Prager yield criterion with zero cohesion

$$\sqrt{II_{\sigma_D}} \geqslant \tau_p p, \tag{7}$$

where II_{σ_D} is the second invariant of the deviatoric stress tensor [45]. The relation (7) states that the material undergoes plastic yielding, when the deviatoric stress is greater than the yield stress. The yield stress plays an important role for the transition of a granular material from a solid (no deformation) to fluid (deformation) state and vice versa, reminiscent of the flow initiation and the deposition process. In two space dimensions the Drucker–Prager yield surface is identical to the Mohr–Coulomb yield surface, and τ_p can be expressed by $\tau_p = \sin\phi$, where ϕ is the internal friction angle and describes the friction between the grains. Note that sometimes the expression $\tau_p = \tan\phi$ is used for the yield stress in the literature (e.g., Moriguchi et al. [16], Oda et al. [46]), which is an approximation and only valid for small internal friction angles. For typical values of ϕ, which are in the order of 30° for granular flows, one should use $\tau_p = \sin\phi$. The pressure dependence of the yield stress causes a higher material resistance against deformations for regions under high pressure. Therefore, the shock front evolution for a flow against an obstacle or a rigid wall is very sensitive to the internal friction angle due to high pressures appearing at or in the vicinity of the wall [6]. The same is true during the deposition process and the flow convergence. As we will see later, the pressure-dependent yield stress is a good rheological model for granular flows considered here. Cohesion can easily be included in model (3) by adding a constant tensile stress τ_c to the total yield stress $\tau_y = \tau_c + \tau_p p$. As we are considering dry granular materials, for simplicity we set $\tau_c = 0$. Note that for slow motion of grains Jop et al. [7] also utilised a pressure-dependent effective viscosity, $\nu_{\text{eff}} = \mu(I)\, p/\|\mathbf{D}\|$, where $\mu(I)$ is the friction coefficient, which depends on the inertial number I. However, in their formulation no linear viscous stress contribution (linear in the strain rate $\|\mathbf{D}\|$) is taken into account ($\nu = 0$) and the strain rate dependence of the stresses is through $\mu(I)$, which is limited by the parameter μ_2 for high values of I. The friction coefficient requires three material dependent constants, which must be determined in experiments on steady uniform flows. In our model, we use the simple relations (4) and (6), in which τ_p is obtained in terms of the internal friction angle, which does not require any fit parameters. This is an advantage.

With the notation

$$\mathbf{F} = \mathbf{g} + (\mathbf{u}\cdot\nabla)\mathbf{u} + \nu\Delta\mathbf{u} + 2\ \text{div}\left(\tau_y \frac{\mathbf{D}}{\|\mathbf{D}\|}\right), \tag{8}$$

the momentum Eq. (2) can now be expressed as (by utilising the continuity Eq. (1))

$$\partial_t\mathbf{u} = \mathbf{F} - \nabla p. \tag{9}$$

Eq. (9) is integrated numerically to compute the velocity field $\mathbf{u}$. A pressure equation is derived by applying the divergence operator on the momentum conservation (9) and using the continuity Eq. (1) to yield:

$$\Delta p = \nabla\cdot\mathbf{F}. \tag{10}$$

As no explicit equation for the pressure is given in the primitive variables formulation (1) and (2), the Eqs. (9) and (10) are solved numerically. Note that $\mathbf{F}$, and hence the right-hand-side of (10), explicitly depend on the pressure for a pressure-dependent yield stress. This leads to a more complicated situation as illustrated in the following. For a pressure-independent yield stress, (10) forms the well-known Poisson equation for the pressure.

2.2. Boundary conditions

The model (1) and (2) must be complemented by appropriate boundary conditions. At every domain border a boundary condition for both the tangential and normal velocity is needed. In rapid flows of granular material down the slopes, even the lowest particle layer in contact with the rigid bottom boundary moves with a non-zero and non-trivial velocity [2,5,17–20]. We use the Coulomb

sliding law to model the interaction of the material with rigid boundaries [15]:

$$T^b = \frac{v^b}{|v^b|} \tan\delta N^b, \tag{11}$$

where T^b is the shear stress, N^b the normal pressure and v^b the velocity at the sliding surface (b). The bed friction angle δ defines the frictional strength. Let $\mathbf{n}$ be the normal vector and $\mathbf{t}$ the tangential vector of the boundary, then the Coulomb sliding law (11) relates the shear stress $T^b = \boldsymbol{\sigma}^b\mathbf{n}\cdot\mathbf{t}$ to the normal pressure $N^b = -\boldsymbol{\sigma}^b\mathbf{n}\cdot\mathbf{n}$ and forms a pressure-dependent velocity boundary condition. For example, the Coulomb sliding law at the bottom boundary with the basal normal vector parallel to the z-direction ($\mathbf{n} = (0,1)^T$, $\mathbf{t} = (1,0)^T$) can be written as

$$v^b_{\text{eff}}\left([\partial_z u]^b - 2c^{\text{F}}[\partial_x u]^b\right) = c^{\text{F}}p^b. \tag{12}$$

Here the 'friction factor' is defined by $c^{\text{F}} = \tan\delta\, u^b/|u^b|$. In deposition processes, i.e., situations, in which the material comes to rest, a discontinuity at $u^b = 0$ appears, which cannot be treated in numerical simulations. Therefore, we use an exponential factor, $[1 - \exp(-m_{c\text{-}}u^b)]$, similar to that for the yield stress, to smooth the friction factor. In Domnik and Pudasaini [15] a pressure-independent yield stress is considered, which means that also v_{eff} does not depend on the pressure and the velocity boundary condition depends linearly on the pressure (12). Here, we consider a pressure-dependent yield stress ($\tau_p \neq 0$), which leads to a non-linear dependency of the velocity boundary values on the pressure, and from (4), (6), and (12) it follows:

$$[\partial_z u]^b = c^{\text{F}}\left(2[\partial_x u]^b + \frac{p^b\|\mathbf{D}\|^b}{v\|\mathbf{D}\|^b + \tau_p p^b}\right). \tag{13}$$

Note that for $\delta = 0$, the friction factor c^{F} also equals zero and the simple free-slip boundary condition is obtained. Also note that Jop et al. [7] use a no-slip boundary condition, but for particle slip along the base a boundary equation like (13) is necessary. At penetrable boundaries the velocity boundary conditions are defined by in- and outflow conditions. This is discussed in more detail later, when we present the coupling of the full two-dimensional with the one-dimensional, depth-averaged model.

For a constant yield stress, $\mathbf{F}$ does not depend on the pressure and consequently the pressure emerges only through a pressure gradient in the momentum Eq. (9). In fact, p appears as a Lagrange multiplier that constrains the velocity field to remain divergence-free and no additional pressure boundary conditions are required. On the contrary, a pressure dependency of the yield stress causes the pressure, p, and its derivatives, $\partial_x p$ and $\partial_z p$, to appear in every vector component of $\mathbf{F}$ in (8), and hence in the momentum Eq. (9) (emerging from the fourth term on the right-hand-side of (8)). Therefore, both pressure and velocity boundary conditions are needed to close the model Eqs. (1) and (2). At rigid boundaries we use a Neumann boundary condition for the pressure by applying the momentum conservation in direction of the boundary normal

$$\mathbf{n}\cdot\nabla p = \mathbf{n}\cdot\mathbf{F}, \tag{14}$$

as often done in defining the boundary conditions for the pressure Poisson equation for a Newtonian fluid [47,48]. Note that the boundary condition (14) cannot be used at penetrable boundaries, where the in- or outflow velocities vary with time. However, if this variation is known, (14) can still be modified appropriately. At penetrable boundaries (interfaces), which occur in the coupling between the full two-dimensional with the one-dimensional model, we will employ in- and outflow conditions for the pressure, which represent a type of Dirichlet boundary conditions. When the coupling with the one-dimensional, depth-averaged model is presented, we will cover this in more detail.

Note that we consider the motion of granular material in a narrow rectangular inclined channel with the main flow direction parallel to the x-axis. In this situation, the shearing at the (smooth) sidewalls has only a marginal influence on the granular flow and can be neglected [5,6].

2.3. Numerical method

The fundamental concepts of our numerical method are based on *NaSt2D* [49], a computer code using the finite-volume method for the simulation of incompressible Newtonian fluids. Following [49,50] , we introduce a staggered grid, in which the velocities and the pressure are not located at the same grid points to avoid possible pressure oscillations. The pressure p is located in the cell centres, the x-velocity u in the midpoint of the vertical cell edges and the z-velocity w in the midpoint of the horizontal cell edges. The spatial derivatives are replaced by centred differences except for the convective terms, which are discretised by using a mixture of central differences and the donor-cell discretisation. To discretise the time derivatives, we use first-order difference quotients. To simulate and visualise the rapid free surface flow of frictional granular material, the marker-and-cell method is applied, in which marker-particles are used to determine whether a cell contains 'fluid' or not [50–52]. The flow depth is then computed from the position of the marker particles. A detailed description of the numerical scheme with applications to inclined channel flows of granular materials is available in Domnik and Pudasaini [15].

As in Domnik and Pudasaini [15], we deduce from the continuity and momentum conservation a second order partial differential equation for the pressure, (10), which is closed by velocity and pressure boundary conditions, (13) and (14). But, different from Domnik and Pudasaini [15], where a pressure-independent yield stress is considered, here the system of equations, formed by (10), (13), and (14), is non-linear in the pressure. We use a modified version of the Powell's hybrid method to solve this non-linear system of equations [53,54].

3. Depth-averaged 1D granular flow model

In the following a depth-averaged, one-dimensional granular flow model and its numerical solution methods are presented.

3.1. Model equations

We consider a simple one-dimensional frictional granular flow model, in which the constitutive behaviour of the granular material is described by a Mohr–Coulomb yield criterion. The Coulomb friction law, (11), is used as bottom boundary condition. By depth-averaging the incompressible equations for conservation of mass and momentum, the following equations are then obtained for the depth-averaged model (DAM) [2,21,22]:

$$\partial_t h + \partial_x(h\bar{u}) = 0, \tag{15}$$

$$\partial_t(h\bar{u}) + \partial_x(h\bar{u}^2) + \partial_x\left(\frac{1}{2}\beta h^2\right) = sh, \tag{16}$$

where $t, x, h, \bar{u}$ are the time, the coordinate along the slope, flow depth, and (depth-averaged) downslope velocity, respectively. The net driving acceleration is given by $s = g\cos\zeta(\tan\zeta - \tan\delta)$ and $\beta = gK\cos\zeta$, where ζ is the slope angle, δ is the bed friction angle, g is the gravity acceleration, and $K_{act/pas} = 2\sec^2\phi\left(1 \mp \sqrt{1 - \cos^2\phi\sec^2\delta}\right) - 1$ is the earth pressure coefficient, in which ϕ is the internal friction angle of the granular

material. Note that K jumps from active (spreading, $\partial_x u > 0$) to passive (contracting, $\partial_x u < 0$) when $\partial_x u = 0$. This can be smoothed by a regularisation process [55]. The term $\partial(0.5\beta h^2)/\partial x$ represents the pressure gradient. The source term, s, is the interaction of the medium with the surrounding, namely the gravity and the basal friction, and it makes the system inhomogeneous.

In deriving (15) and (16), the assumption of shallowness of the granular avalanche is implemented. For this purpose the physical variables are non-dimensionalised by using the scalings [2]

$$(x, z, t) = \left(L\hat{x}, H\hat{z}, (L/g)^{1/2}\hat{t}\right), \tag{17}$$

$$(u, w) = (gL)^{1/2}(\hat{u}, \varepsilon\hat{w}), \tag{18}$$

where the hats represent non-dimensional variables, L is a characteristic length, and H is a characteristic height of the flow. The aspect ratio of the granular avalanche is defined as $\varepsilon = H/L$ and assumed to be small. The model equations are correct to order higher than ε.

The Eqs. (15) and (16) comprise a hyperbolic system with the characteristic velocities $\lambda_\pm = \bar{u} \pm \sqrt{\beta h}$ (if K does not switch from active to passive or vice versa). If both characteristic velocities have the same sign, the flow is called supercritical (i.e., $\bar{u}/\sqrt{\beta h} > 1$). If the characteristic velocities have opposite sign, the flow is called subcritical (i.e., $\bar{u}/\sqrt{\beta h} < 1$). When the flowing material is stopped by an obstacle or wall, a previously supercritical flow becomes subcritical, and a shock wave is generated. We consider the depth-averaged model in regions, where ε is small and the flow is in a supercritical state. Otherwise a full two-dimensional model presented in Section 2 is used.

3.2. Numerical method

In applications the depth-averaged model is successfully solved by a higher-order non-oscillatory central (NOC) total variation diminishing (TVD) differencing scheme mainly with the Minmod TVD limiter [2,6,23,18,56,57]. The concept of flux limiters allows to switch between high and low resolution schemes by considering the ratio r of successive gradients of the field variables on the solution mesh. With this higher-order method spurious oscillations induced by high resolution schemes can be avoided by using a low resolution scheme if the ratio r becomes large. The disadvantage of this concept, however, is that the ratio r also becomes large and even negative near extrema and a low-resolution scheme is used in these situations. We observed in simulations that for inflow conditions (at the interface between 2D and 1D regions), which do not vary strictly monotonically with time, even this can be a source for spurious oscillations. As we are considering the depth-averaged model in regions, where the flow is supercritical and no sharp wave fronts occur, we can use a high resolution scheme and do not need to introduce the concept of flux limiters. For this reason, we numerically solve the one-dimensional granular flow model by implementing a second-order non-oscillatory central differencing scheme which is based on the beam-warming method [2,58] . This turns out to work very well for our particular problem.

4. Coupled model

In the coupled model the two-dimensional Coulomb-viscoplastic granular flow model with pressure-dependent yield stress is used in regions with a strong full two-dimensional flow characteristic and the depth-averaged, one-dimensional granular flow model in regions with negligible momentum transfer in z-direction. Here, we propose a domain decomposition strategy of the computational domain in 2D and 1D regions and suggest appropriate boundary conditions at the interfaces, which separates these regions.

4.1. Domain decomposition

The computational complexity and cost can be dramatically reduced by using the one-dimensional granular flow model in regions with smooth changes of flow variables. In regions where depth-averaging becomes inaccurate, like in initiation and deposition regions, and also in flow converging and diverging regions, in particular when the flow hits an obstacle or a defence structure, the two-dimensional Coulomb-viscoplastic model is used. The regions in which the 2D (1D) model is used are called 2D (1D) regions. In Fig. 2 a possible domain decomposition is sketched for the channel flow illustrated in Fig. 1. The full two-dimensional model provides the flow velocities u, w, along x- and z-directions and the pressure p. The flow heights can be obtained by considering the position of the marker particles used in the MAC method. The one-dimensional model supplies the depth-averaged velocity $\bar{u}$ and the flow height h.

To determine whether the one-dimensional model is valid at a given position in the channel, we introduce the shallowness parameter, $\varepsilon = |w|/|u|$, as the ratio of the velocity normal to the channel (w) to the velocity along the channel (u). The shallowness parameter is equivalent to the aspect ratio H/L, since w scales with UH/L, where U is a typical velocity, which defines the scale for u, compare (18). If ε is small ($\varepsilon \ll 1$), the momentum transfer in the flow depth direction is much smaller than the momentum transfer along the downslope (channel) direction and depth-averaging is legitimate. Hence, the interfaces, which separate the 2D and 1D regions, should be located at positions where the shallowness parameter is sufficiently small. Here, we propose two different strategies of domain decompositions: (i) The interface position can be set automatically during runtime by computing the shallowness parameter at every position in the channel. However, for 1D–2D interfaces this approach is not straightforward as usually the 2D-subdomain has to be enlarged with time due to the evolution of a shock wave like for a flow against an obstacle. This requires the computation of the two-dimensional model in areas where the one-dimensional model was used previously. (ii) In contrast, for simplicity we can consider static interfaces, whose position can be fixed a priori. One possibility is to carry out the domain decomposition a priori, essentially driven by experience, physical and geometrical considerations. Alternatively, an a priori estimate of the interface position can be obtained in a much better and dynamic way by performing a foregoing, fast simulation with the one-dimensional model, from which the shallowness parameter is estimated by $\varepsilon = 1/Fr^2$, where $Fr = u/\sqrt{\beta h}$ is the Froude

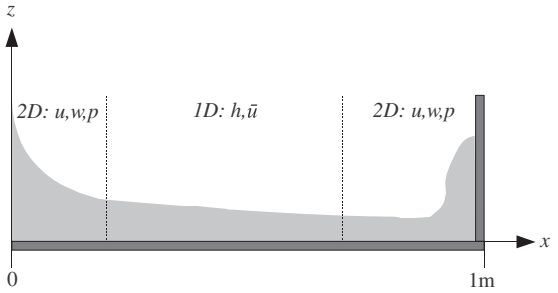

Fig. 2. A possible domain decomposition and the associated field variables for flow along an inclined channel closed by a perpendicular wall at $x = 1$ m downstream. The 2D model supplies the velocities u, w, and the pressure p. The 1D model provides the flow depth h and the depth-averaged downslope velocity $\bar{u}$. The dotted lines indicate the 2D–1D, 1D–2D, interface, respectively.

number. As from dimensional analysis, (17) and (18), it follows that $1/Fr^2$ is equivalent to ε. However, due to the limited validity of the one-dimensional model, this provides only a rough estimate and the length of two-dimensional subdomain must be chosen somewhat greater than suggested by the one-dimensional simulation.

4.2. Boundary conditions for DAM at the interface

The one-dimensional granular flow model requires boundary conditions for the flow height and the mean velocity at the interface. We obtain them from the corresponding values of two-dimensional Coulomb-viscoplastic model as follows:

$$u^{1D}(t, x = x_{IF}) = \bar{u}^{2D}(t, x = x_{IF}), \tag{19}$$

$$h^{1D}(t, x = x_{IF}) = h^{2D}(t, x = x_{IF}), \tag{20}$$

where x_{IF} is the interface position, and depth-averaging is defined by

$$\bar{u}(t, x) = \frac{1}{h}\int_0^h u(t, x, z)dz. \tag{21}$$

However, in the one-dimensional model a staggered grid is used, where the boundaries of the cells at the new time level are the centres of the cells at the old time level. This time-staggered grid is a central concept of NOC schemes. On the contrary, a space-staggered grid, which does not move with time, is considered in the full two-dimensional model. These different numerical grids for the 1D and 2D model have to be taken into account properly, when setting the boundary conditions at the interface for both the 1D and the 2D model.

4.3. Boundary conditions for N-DAM at the interface

The treatment of the boundary conditions for the two-dimensional model is much more complex than for the one-dimensional model, because two-dimensional quantities have to be determined from one-dimensional ones. The two-dimensional Coulomb-viscoplastic model requires boundary conditions at the interface both for the velocities u and w and the pressure p. In an intuitive first approach one can think about setting the channel parallel velocity equal to the depth-averaged one-dimensional velocity and the velocity in the flow depth direction equal to zero at the interface:

$$u^{2D}(t, x = x_{IF}, z) = u^{1D}(t, x = x_{IF}), \tag{22}$$

$$w^{2D}(t, x = x_{IF}, z) = 0. \tag{23}$$

However, this causes several problems. At first, it is by no means clear how to set appropriate pressure boundary conditions such that the continuity equation is fulfilled in the whole N-DAM domain. The Neumann pressure boundary condition which is used at rigid boundaries, (14), cannot be used at penetrable boundaries with time-dependent in- or outflow conditions. Secondly, the variation of the u velocity with depth is assumed to vanish, which is actually not the case near the base for bed friction angles $\delta > 0$. Indeed, the shearing of the material should be small at the interface, but using a u velocity constant with depth produces non-smooth velocities and pressures at the interface due to an acceleration of the material near the bottom and a deceleration of the material near the free surface. Furthermore, there is no physical justification for setting the w velocity to zero even if it is small compared to the u velocity. Instead, it contradicts with the continuity requirement, because $\partial_x u \neq 0$ in general. Therefore, we cannot use (22) and (23) as proper boundary conditions at the interface. Rather, we propose the following natural and legitimate relations at the interface:

$$\bar{u}^{2D}(t, x = x_{IF}) = u^{1D}(t, x = x_{IF}), \tag{24}$$

$$\partial_x \partial_z u^{2D} = 0, \tag{25}$$

$$p^{2D}(t, x = x_{IF}, z) = p^{1D}(t, x = x_{IF}, z), \tag{26}$$

$$\partial_x u^{2D} + \partial_z w^{2D} = 0. \tag{27}$$

Eqs. (24) and (25) define the channel parallel velocity at the interface, which varies with flow depth. The assumption $\partial_x \partial_z u = 0$ is not a strong constraint, because in the vicinity of the interface the momentum change in the flow depth direction is small. The isotropic pressure (defined by the trace of the stress tensor) is given by $p^{1D} = g\cos\zeta(h - z)(1 + K)/2$ in the one-dimensional model [2]. Eq. (27) represents the continuity equation. With the boundary conditions at the interface, (24)–(27), the continuity requirement is fulfilled in the whole N-DAM domain and no artificial acceleration or deceleration of the material at the interface is introduced.

5. Performance of coupled model

First, we demonstrate the performance and present an error analysis of the coupled 2D/1D/2D model. For this purpose two different setups are considered: (i) an undisturbed inclined channel flow (Setup I), and (ii) a flow hitting a perpendicular wall (Setup II). Subsequently, the correspondence of the material parameters in the two- and one-dimensional models are investigated. Furthermore, the impact of the interface position on the numerical results is illustrated.

Some experimental results, depth-averaged exact solutions, and depth-averaged numerical simulations for rapid granular flows hitting and flowing around an obstacle can be found in Gray et al. [25] and Cui and Gray [32]. These results are relevant to flows analysed in Sections 5.1.1 and 5.1.2, respectively.

We simulate a rapid flow of granular material down a channel with an inclination of $\zeta = 50°$, which is continuously fed from a silo, see Fig. 1. The inlet height is $h_{in} = 6$ cm, and the mean inlet velocity is $\bar{u}_{in} = 0.37\ \mathrm{ms}^{-1}$. The internal friction angle is set to $\phi = 33°$, the bed friction angle to $\delta = 22°$, and the kinematic viscosity to $\nu = 0.003\ \mathrm{m}^2\ \mathrm{s}^{-1}$. These flow configurations are similar to those used in Pudasaini et al. [5], Pudasaini and Kröner [6], Domnik and Pudasaini [15] and Pudasaini and Domnik [37]. In Setup I the channel has a length of $L = 1.5$ m and at the end of the channel an open end outflow condition is considered. In Setup II we consider a channel of length $L = 1$ m, which is closed by a rigid perpendicular wall.

5.1. Model assessment

At first, we simulate the channel flow in a rectangular domain $\Omega = [0, L] \times [0, H]$ with the full two-dimensional model, where L is the channel length and H is an appropriately chosen domain height. Secondly, we divide the whole domain in three sub-domains $\Omega_1 = [0, 0.2] \times [0, H]$, $\Omega_2 = [0.2, 0.7] \times [0, H]$ and $\Omega_3 = [0.7, L] \times [0, H]$. In Ω_1 and Ω_3 we use the full two-dimensional model as required by the physics of the flow, whereas in Ω_2 the depth-averaged model is used, because here the momentum transfer in the flow depth direction is negligible. This coupled-simulation is an approximation of the full two-dimensional simulation.

5.1.1. Setup I: Undisturbed flow

In Setup I, we consider an undisturbed flow by setting L to a sufficiently large value ($L = 1.5$ m). In Fig. 3 the simulated velocity field, $|\mathbf{u}| = \sqrt{u^2 + w^2}$, with the coupled 2D/1D/2D model is presented for a time $t = 0.75$ s. The flow enters the channel at $x = 0$. The 2D–1D interface is located at $x = 0.2$ m and the 1D–2D interface is located at $x = 0.7$ m (indicated by the grey vertical lines). Both the velocity and the flow depth show smooth transitions at

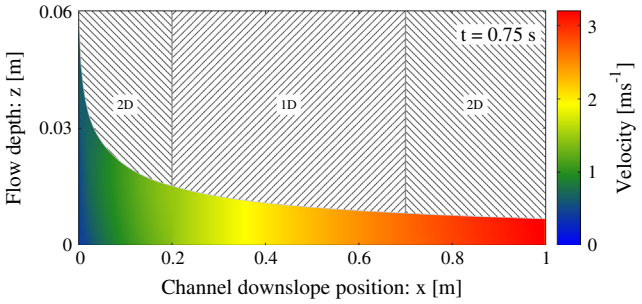

Fig. 3. Simulation of the velocity field, $|\mathbf{u}| = \sqrt{u^2 + w^2}$, and flow depth of an undisturbed flow with the coupled 2D/1D/2D model. The flow enters the channel at $x = 0$. The 2D–1D interface is located at $x = 0.2$ m and the 1D–2D interface is located at $x = 0.7$ m (indicated by the grey vertical lines).

each interface. Although the flow is very shallow in the third sub-domain Ω_3, the two-dimensional model is used there, to study the performance of the coupled model for a 1D–2D interface. This becomes important when high momentum transfer in the flow depth direction are expected in this region like in Setup II, where a flow down a channel closed by a perpendicular wall is considered.

The evolution of the velocity vectors with time is shown in Fig. 4. There is a strong velocity shearing through the flow depth in the vicinity of the silo inlet in the Ω_1 (2D) subdomain. With our choice of boundary conditions for the two-dimensional model, shearing through depth is taken into account. This is a big advantage as shearing near the base is not negligible and the usage of an inflow velocity constant with depth would not be appropriate at the interface, compare Fig. 5. Ultimately, the absence of reflections at the sub-domain boundaries confirms the physical significance of our choice of boundary conditions. In Fig. 6 the flow depth and mean (depth-averaged) downslope velocity simulated with the coupled 2D/1D/2D model are compared with ones simulated with the full two-dimensional model. We define the relative error of the coupled simulation by $r = |v^{coupled} - v^{2D}|/|v^{2D}|$ for a physical variable v simulated with either the full two-dimensional model (v^{2D}) or the coupled model ($v^{coupled}$). The relative error for the coupled 2D/1D/2D simulation is below 2% for both the flow depth and the mean velocity. This marginal error justifies the coupling of the two-dimensional Coulomb-viscoplastic model with the one-dimensional model, based on the Mohr–Coulomb yield criterion.

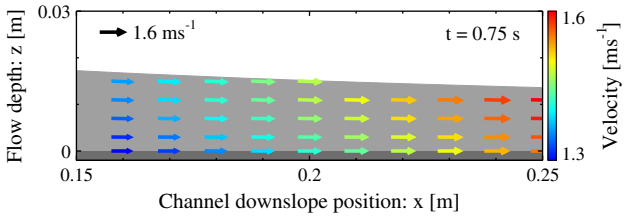

Fig. 5. Velocity field simulated with the full two-dimensional model around $x = 0.2$ m, which corresponds to the 2D–1D interface in the coupled simulation.

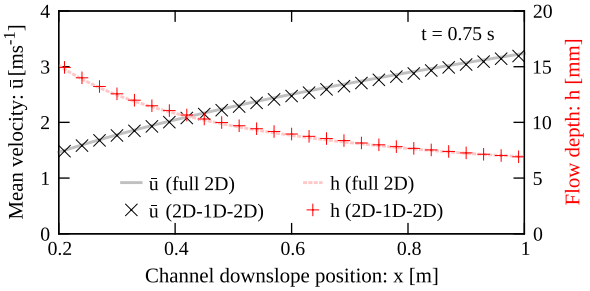

Fig. 6. Mean downslope velocity and height at $t = 0.75$ s for an undisturbed flow simulated with the full 2D model (lines) and the coupled 2D/1D/2D model (symbols). The 2D–1D interface is located at $x = 0.2$ m and the 1D–2D interface at $x = 0.7$ m, respectively.

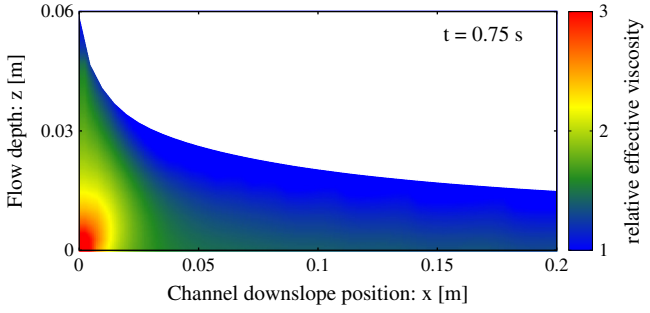

Fig. 7. Ratio of effective viscosity to constant viscosity, ν_{eff}/ν, near the inlet.

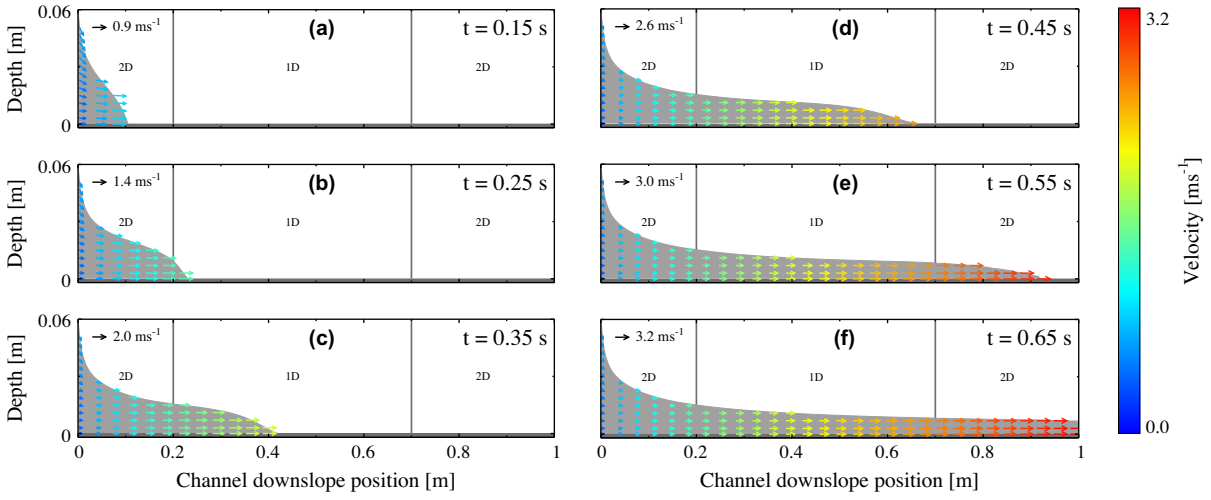

Fig. 4. Snapshots of velocities (arrows) and depth evolutions (background grey) in rapidly flowing granular material down a steep rectangular open channel simulated with the coupled 2D/1D/2D model.

Note that although we choose a relatively low value for the viscosity ν, its contribution to the effective viscosity ν_{eff} is not negligible. This is exemplarily demonstrated in Fig. 7 for the flow near the inlet. Here the ratio of the effective viscosity to the constant viscosity, ν_{eff}/ν, is shown. Fig. 7 demonstrates that ν_{eff} is of the same order of magnitude as ν for the flow near the inlet. In regions away from the silo gate and close to the free surface, where pressure is small, the effective viscosity is primarily given by ν.

5.1.2. Setup II: Flow against wall and deposition

A critical point in coupling models of different dimensions is the step moving from the lower dimensional (depth-averaged) model to the higher dimensional (full, non-depth-averaged) model as carried out at the 1D–2D interface. It is desired to recapture the higher dimensional properties of the flow on the flow variables when the flow changes its behaviour, e.g., from a supercritical to a subcritical state. This transition is characterised by a substantial momentum transfer in the flow depth direction. This is particularly interesting in view of flows hitting obstacles, where depth-averaging becomes largely inaccurate and a high momentum transfer in z-direction (perpendicular to the channel) evolves. This is demonstrated in Fig. 8, where the time evolution of the velocity field, $|\mathbf{u}| = \sqrt{u^2 + w^2}$, and of the flow depth are shown for a granular flow hitting a perpendicular wall. In the following, the behaviour of the granular material in the vicinity of the wall is considered in more detail.

In Fig. 9a the velocity field, $|\mathbf{u}| = \sqrt{u^2 + w^2}$, near a perpendicular wall, simulated with the coupled model, is presented at different time steps. As soon as the flow hits the wall it is decelerated and a strong velocity shearing through the depth and along the channel is simulated as observed in experiments [5]. A deposition region is quickly formed, in which the material is nearly at rest and exhibits solid-like characteristics. In the course of time, the fluidised region, where a strong shearing is observed, shrinks and the deposition region grows, as new arriving material is stopped by the already accumulated, resting mass. Note that we consider here a relatively short time range (≈0.15 s) after the material has hit the wall, where the velocity of the arriving material is still high and hence causes an increasing deposit height at the wall when climbing up the resting material. Fig. 9b shows the associated pressure field. The dynamic pressure obtains its maximum value, when the flow is hitting the wall, as a result of the extremely strong deceleration of the material near the wall. As in Pudasaini et al. [5] we define the shock front position as the position, where new arriving mass hits already stopped material. As the shock front position moves in the upstream direction, the pressure decreases slightly with time and is more and more generated by the load of the accumulated material. Note that the pressure distribution along the depth is not linear in the deposit. Hence, it cannot be described by a linear hydrostatic pressure, which is used in classical avalanche and granular flow models. In particular, the hydrostatic pressure underestimates the full dynamic pressure. For example, at $t = 0.75$ s the dynamic pressure at the bottom is $p = 2.3$ kPa, and the hydrostatic pressure is calculated as $p_H = 1.0$ kPa (for $h = 0.11$ m), which is much smaller than p.

The yield stress is essential in the description of a flow against a wall as a transition of a fluid to a solid state takes place. Here, we considered a pressure-dependent yield stress, which causes the

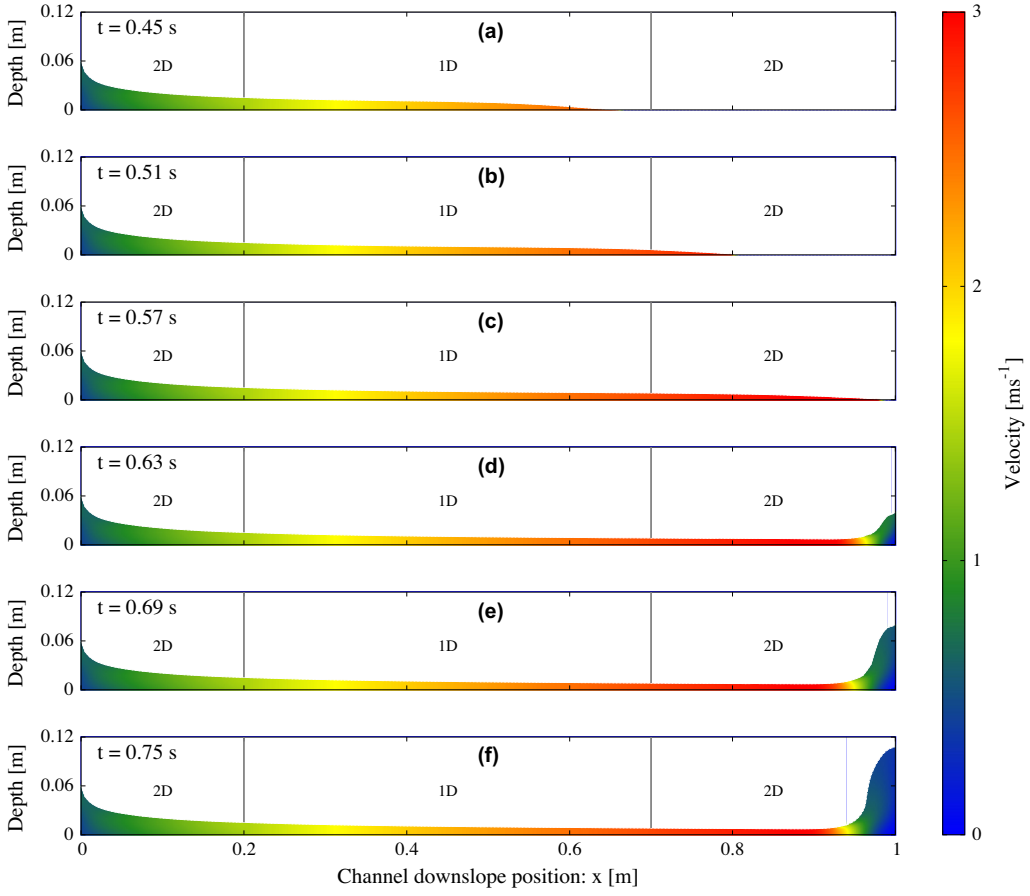

Fig. 8. Snapshots of the evolution of the velocity, $|\mathbf{u}| = \sqrt{u^2 + w^2}$, and flow depth along the entire channel and simulated with the coupled 2D/1D/2D model. The flow enters the channel at $x = 0$. The 2D–1D interface is located at $x = 0.2$ m and the 1D–2D interface is located at $x = 0.7$ m (indicated by the grey vertical lines). At $x = 1$ m a perpendicular wall is erected.

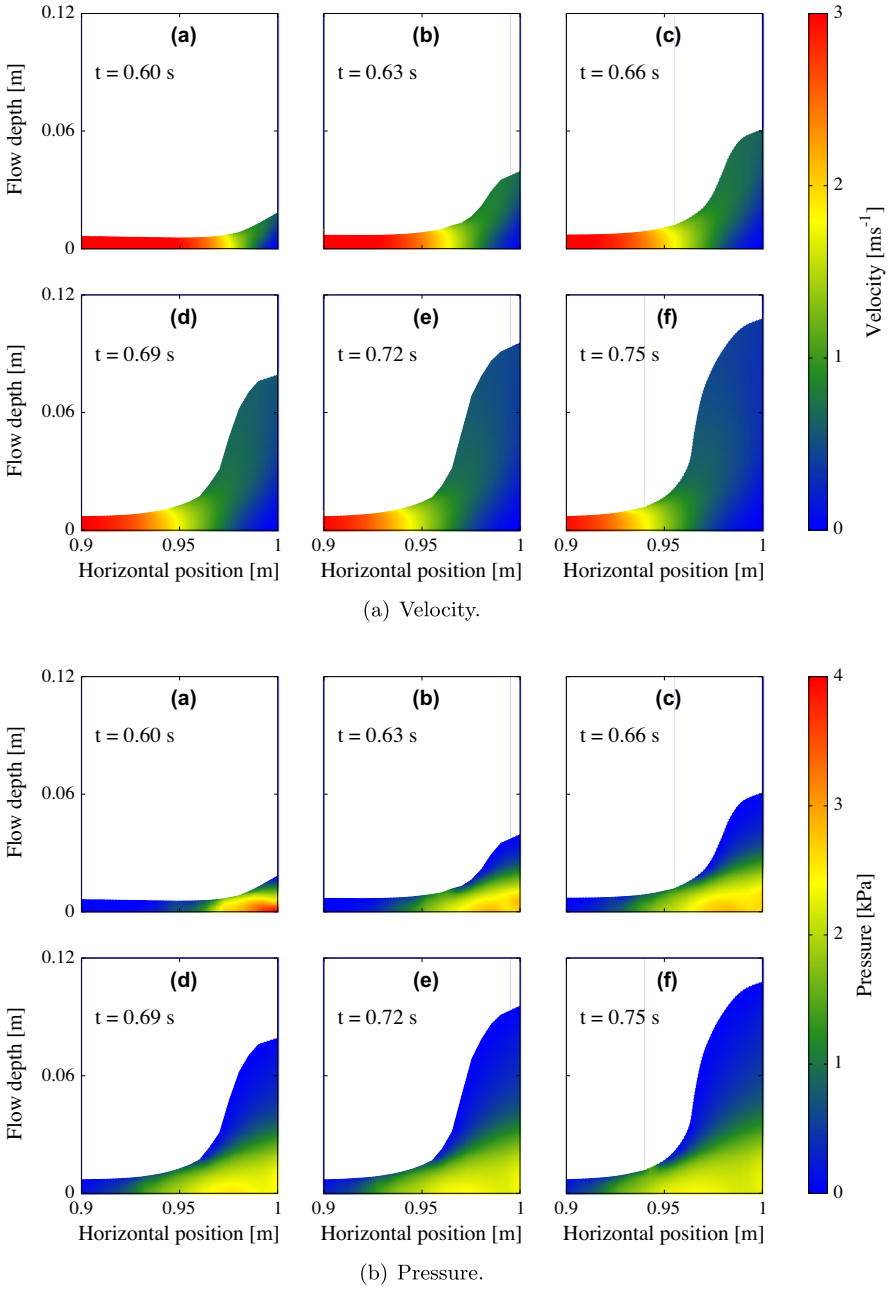

Fig. 9. Snapshots of the evolution of the velocity, $|\mathbf{u}| = \sqrt{u^2 + w^2}$, pressure p and flow depth in the vicinity of a perpendicular wall erected at $x = 1$ m and simulated with the coupled 2D/1D/2D model for a granular material with pressure-dependent yield stress $\tau_y = \tau_p p$ with $\tau_p = \sin\phi$.

relatively high pressure in the vicinity of the wall to amplify the deceleration of the flow, as the effective viscosity increases. This is not the case for a Bingham-type material (pressure-independent τ_y). In Fig. 10 the simulated velocity field, $|\mathbf{u}| = \sqrt{u^2 + w^2}$, and the associated pressure field near a perpendicular wall are shown for a Bingham material with $\tau_y = 100$ Pa. The deceleration of the material by the wall is much less compared to a material with a pressure-dependent yield stress (Fig. 9a). Instead, the wall mainly induces a change of the flow direction to align along the wall. The material climbs up the wall and only a very small deposition region in the corner between the wall and the channel bottom is developed. The pressure (Fig. 10b) in this region is much higher (≈6 kPa) than the pressure as modelled by a pressure-dependent yield stress material (≈4 kPa, Fig. 9b). Therefore, a Bingham material shows a completely different flow behaviour when hitting a perpendicular wall as a pressure-dependent yield stress material. This is an evidence for the significance of a pressure-dependent yield stress, used here, in description of a flow hitting a wall. Furthermore, the results for a pressure-dependent yield stress are in line with our physical intuition and some experimental observations [5].

In order to investigate the accuracy of the coupled simulation, the depth-averaged (mean) velocity and flow height simulated with the coupled model are compared with the ones simulated with the full two-dimensional model in Fig. 11. In vicinity of the wall, the mean velocity decreases rapidly and a shock wave is formed. Both the mean downslope velocity and the flow height, simulated with the full two-dimensional model, are well recaptured by the coupled model. Close to the wall the deviation between the coupled and the full two-dimensional solution

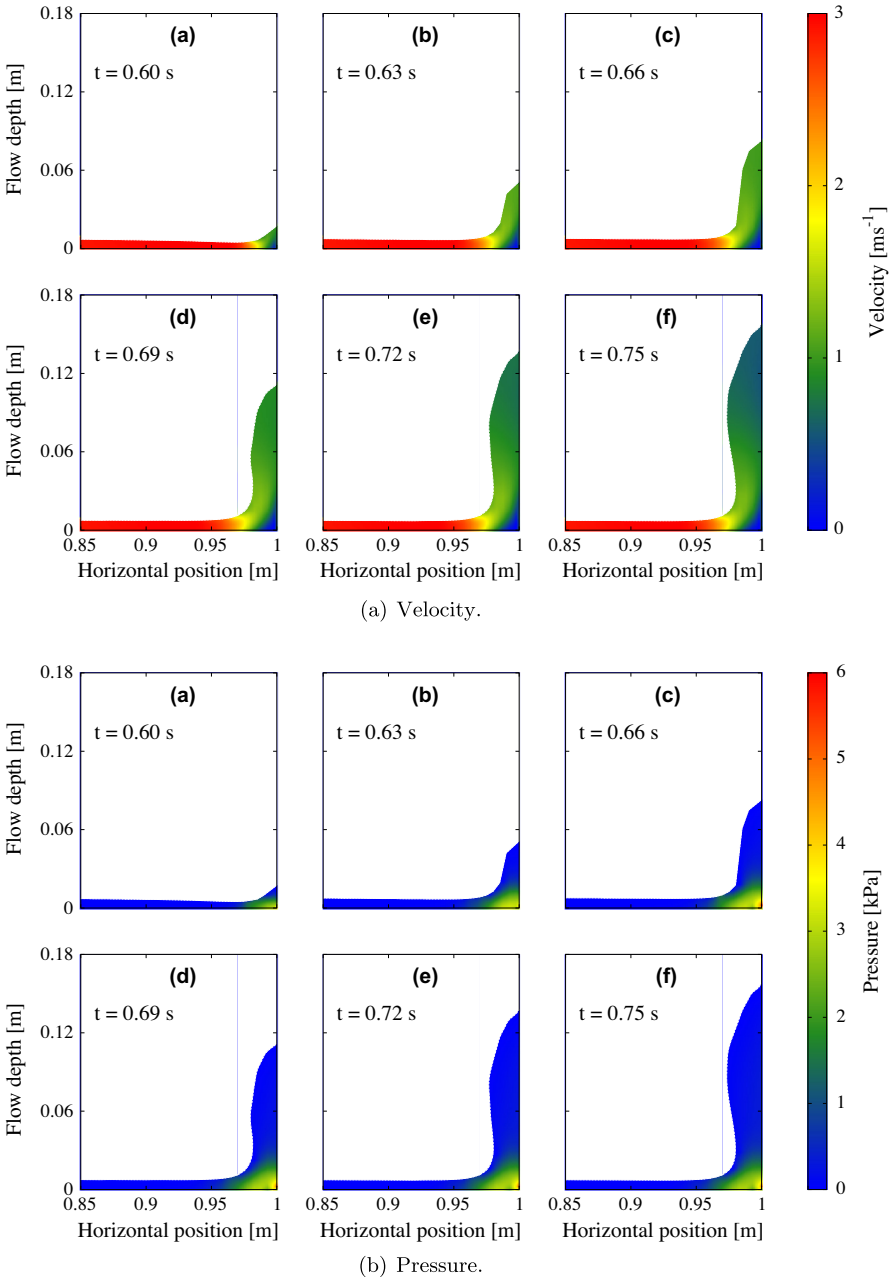

(a) Velocity.

(b) Pressure.

Fig. 10. Snapshots of the evolution of the velocity, $|\mathbf{u}| = \sqrt{u^2 + w^2}$, pressure p, and flow depth in the vicinity of a perpendicular wall erected at $x = 1$ m and simulated with the coupled 2D/1D/2D model for a Bingham material with a pressure-independent yield stress $\tau_y = 100$ Pa.

increases. This is a consequence of the completely different treatments of the free surface in the 2D and 1D model. In the depth-averaged model the flow height is a field variable, whereas in the full two-dimensional model the free surface is determined by the MAC method. This leads to different descriptions of the front shape of the granular avalanche. Again, Fig. 11 demonstrates that our coupling strategy works very well even for sudden changes of flow variables leading to high momentum transfer, energy dissipation and velocity shearing in the flow depth direction.

It is very important to note that by splitting the domain in different subdomains and appropriately using the coupled model instead of a full two-dimensional model, the simulation run-time can be reduced from days to hours for the configurations considered here. The computational cost is mainly affected by the solution of the nonlinear system of equations for the pressure and velocity boundary conditions in the full two-dimensional model, which is very time-consuming for large domains. In general, the running time depends on several factors like grid resolution, domain decomposition, available computing power and more. However, we expect that in most applications the coupled model provides a significant improvement with respect to the computational effort.

Simulation results presented in Figs. 9–11 show that the physical–mathematical models and simulation methods adopted and developed here are capable of capturing shock phenomena in rapid granular flows once the flow hits a rigid wall. Another important aspect in our modelling and simulation approach is that, no assumptions are made both in the physical modelling and the numerical simulation scheme in contrast to the depth-averaged modelling and simulation, where a shallowness parameter is

introduced, hydrostatic pressure, flux limiting and lateral pressure coefficients are assumed. Moreover, full dimensional modelling proposed here avoids the necessity of the inclusion of the earth pressure coefficient as we do not need to close the lateral pressure. Note that in the depth-averaged model simulations, the discontinuity of the pressure coefficient may cause several problems when the flow switches from expanding mode ($\partial_x u > 0$) to diverging mode ($\partial_x u < 0$). The shock-capturing property, the earth pressure coefficient and flux limiting are not required as in depth-averaged modelling, which presents a substantial and genuine advancement.

5.2. Correspondence of material parameters

The interaction of the sliding mass with the basal surface is described by the Coulomb friction law for both the two-dimensional and one-dimensional granular flow models, considered here. However, the implementation of this sliding law is completely different for both models. In the full two-dimensional model the Coulomb friction law represents a pressure-dependent velocity boundary condition, which also defines the pressure near the base by complementing the pressure Eq. (10). In the one-dimensional model the Coulomb friction law emerges in the source term due to depth-averaging and defines the net driving acceleration, (16). To study the correspondence of the Coulomb friction angle in the two-dimensional model (δ^{2D}) with the friction angle in the one-dimensional model (δ^{1D}), we consider an undisturbed channel flow and split the whole domain in one 2D- and one 1D-subdomain. The two-dimensional model is used in $\Omega_1 = [0, 0.2] \times [0, H]$ and the one-dimensional model is used in $\Omega_2 = [0.2, L] \times [0, H]$. The coupled model is solved numerically with two different bed friction angles. In Ω_1 we assume a bed friction angle of $\delta^{2D} = 22°$ and in Ω_2, where the one-dimensional model is used, we consider different bed friction angles δ^{1D} deviating from δ^{2D}. In Fig. 12 the relative error of the mean velocity is considered for different values of $\delta^{1D} = 14°, 18°, 22°, 26°$ and $30°$. It is demonstrated that a deviation of δ^{1D} with respect to δ^{2D} can cause a relative error of several percentages, if the bottom friction in the 1D region is either too strong ($\delta^{1D} > \delta^{2D}$) or too weak ($\delta^{1D} < \delta^{2D}$). Therefore, we conclude that the bed friction angle used in the one-dimensional model well corresponds to the one in the two-dimensional model. Importantly, this implies that the usage of the Coulomb sliding law in the two-dimensional model is essential. No-slip or free-slip boundary conditions (see Domnik and Pudasaini [15]) at the basal surface are not appropriate in coupling with the one-dimensional granular flow model used here. Note that both the bed friction angle and the internal friction angle are used in the two- and also in the one-dimensional model to describe the granular nature of the material. However, since the internal friction angle mainly effects the deposit [6], where depth-averaging is not appropriate, it does not make any sense to consider a correspondence for the internal friction angle.

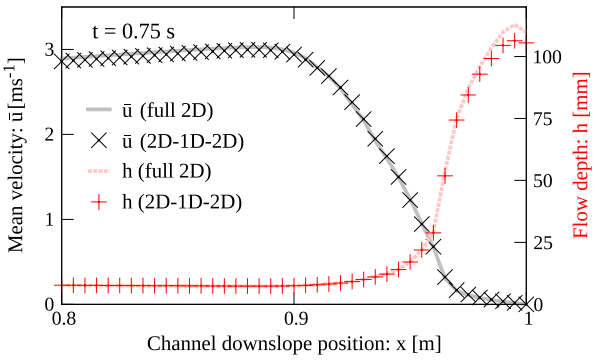

Fig. 11. Mean velocity and height at $t = 0.75$ s for a flow against a perpendicular wall erected at $x = 1$ m, simulated with the full 2D model (lines) and the coupled 2D/1D/2D model (symbols).

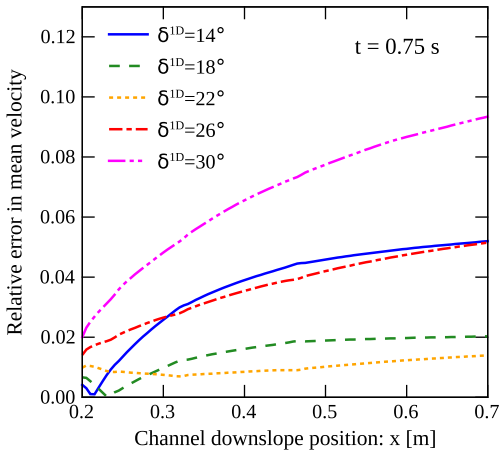

Fig. 12. Relative error of the mean velocity simulated with the coupled 2D/1D model, where the bed friction angle in the 1D subdomain (δ^{1D}) is set independently of the one in the 2D subdomain ($\delta^{2D} = 22°$).

5.3. Interface location

In the vicinity of the silo inlet there is a high momentum transfer in z-direction due to gravitational acceleration. Fig. 13 shows the simulated w velocities near the silo inlet at $x = 0$. The flow shears and spreads rapidly just below the silo gate, while it remains almost unchanged in the further downstream locations. The shallowness parameter, defined as $\varepsilon = |\bar{w}|/|\bar{u}|$, indicates that close to the silo inlet the w velocity component is of the same order as the u velocity component, Fig. 13b. At some distance from the inlet (few centimetres downstream), the w component becomes negligible. This trend is also confirmed by the shallowness parameter, expressed in terms of the Froude number $\varepsilon = 1/Fr^2$, obtained by a fast simulation of the one-dimensional model for an a priori estimate of the interface position. Note that the shallowness parameter appears in the dimensional analysis of the depth-averaged equations and is an ordering parameter. Therefore, the knowledge of its exact value is not required and it is natural that different approaches lead to slightly different results. This explains that the shallowness parameter estimated by the Froude number differs slightly from the one computed by the velocity ratio in Fig. 13b. The important message here is that in regions with high momentum transfer in the flow depth direction, depth-averaging is not valid and the full two-dimensional model must be used.

To study the impact of the interface position, which separates the 2D and 1D model, we simulate the coupled model with different interface positions $x_{IF} = 2$ cm, 4 cm, 6 cm and 10 cm. We define the global velocity average by $\tilde{u}(l) = 1/l \int_0^l \bar{u} dx$, where $\bar{u}$ is defined by (21). Here, we use $l = 0.2$ m, as we focus on the flow in the vicinity of the silo inlet. In Fig. 14 the relative error of the averaged velocity $\tilde{u}$ (0.2 m) is presented for different interface positions with respect to time. In the beginning, when the flow passes the respective interface, the relative error is on the order of 10% up to 40%, depending on the interface position. This error is mainly due to the previously mentioned different front shapes in the 1D and 2D model (compare the simulated flow depth shown in the inset of Fig. 14). The one-dimensional model produces a strong diffusive flow front in contrast to the one generated by the MAC method in the two-dimensional model. After some time, the fluid front moves beyond the considered range for averaging and the relative error drops to only few percentages for interface positions $x_{IF} \geqslant 4$ cm and to roughly 15% for $x_{IF} = 0.2$ cm respectively. Two

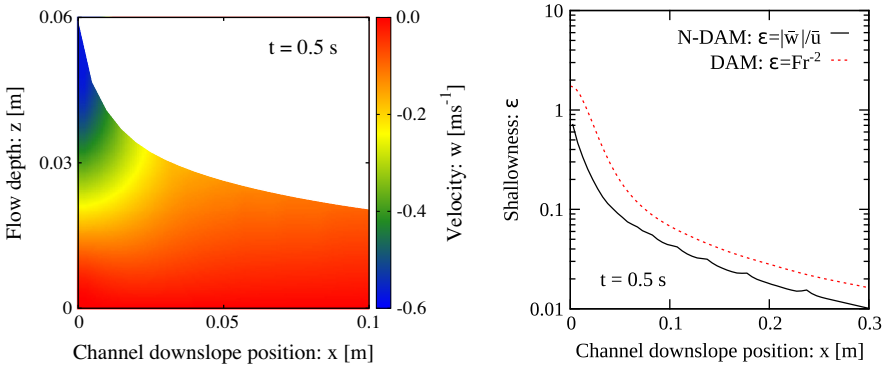

(a) The w velocity in flow depth direction. (b) Shallowness parameter.

Fig. 13. Simulation of the velocity component in the flow depth direction (w) and shallowness parameter, ε, in the vicinity of the silo inlet (located at $x = 0$). In the full two-dimensional model (N-DAM) ε is computed by the velocity ratio $|\bar{w}|/\bar{u}$. In the depth-averaged one-dimensional model (DAM) the shallowness parameter is estimated by $\varepsilon = 1/Fr^2$, where Fr is the Froude number.

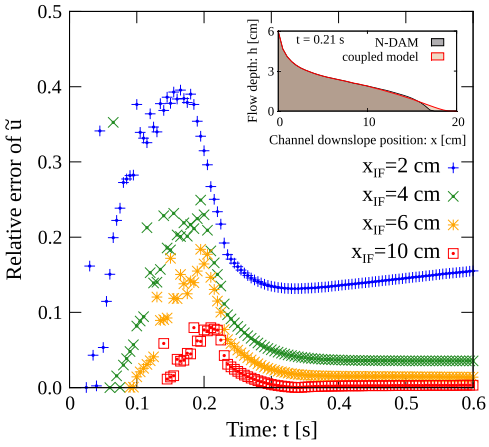

Fig. 14. Relative error of the globally averaged velocity $\tilde{u}$ evolving with time for different interface positions x_{IF}. In the inset, the flow depth is shown for the coupled and the full two-dimensional model. The 2D–1D interface position of the coupled model in the inset is located at $x_{IF} = 0.1$ m.

important observations can be deduced from Fig. 14: First, if the interface positions are not appropriately chosen, this can increase the inaccuracy of the coupled simulation dramatically. Second, for appropriately chosen interface locations, the relative error is not increasing with time. This means that the coupled and full two-dimensional model do not diverge with time. By comparing Figs. 13b and 14 we conclude that $\varepsilon < 0.1$ is a minimum requirement at the interface position, in order to get a reasonable accuracy of the coupled simulation. Thus, we suggest to use this requirement in the mentioned a priori estimate of the interface position. However, there is no strict rule for fixing the interface position and it is always a compromise between accuracy of the solution and computational cost.

6. Summary

We developed a full two-dimensional Coulomb-viscoplastic model for inclined channel flows of granular material that comes to rest once the flow hits a perpendicular wall in the downstream. The presented model includes the basic features and observed phenomena in dense granular flows like the exhibition of a yield strength and a non-zero slip velocity. We proposed a pressure-dependent yield strength to account for the frictional nature of granular materials. The yield strength is uniquely defined by the internal friction angle of the material and no additional calibration parameter is required as, e.g., for Bingham materials, which is a big advantage. We demonstrated that the pressure-dependent yield strength plays an important role in deposition processes. A Bingham-type material (pressure-independent yield stress) shows a completely different flow behaviour when hitting a perpendicular wall. For this type of flow, the wall mainly induces a change of the flow direction rather a development of a deposition region. In the proposed model, the interaction of the flow with the solid boundary is modelled by a pressure and rate-dependent Coulomb-viscoplastic sliding law. The bed friction angle defines the frictional strength and depends on both the granular material and the boundary substrate. As the sliding law has a substantial impact on the overall flow behaviour, a physically reasonable description of the bottom friction is very essential. Hence, the presented full two-dimensional Coulomb-viscoplastic granular flow model, characterised by the internal and bed friction angle, constitutes a substantial advancement to the existing models.

Additionally, we presented a novel multiscale and multiphysics strategy to couple the full two-dimensional, non-depth-averaged model (N-DAM) with a one-dimensional, depth-averaged model (DAM) for rapid motions of frictional granular materials. With the coupled model the computational complexity can dramatically be reduced by using DAM in regions with smooth changes of flow variables. In regions where depth-averaging becomes inaccurate, like in the initiation and deposition regions and particularly, when the flow hits an obstacle or a defence structure, N-DAM must be used. With this, we retain the essential physics of the flow. This is a substantial advantage when considering large scale geophysical mass flows in nature such as snow avalanches, rock avalanches and debris flows. We presented different strategies for a suitable domain decomposition and propose an a priori estimate of the interface position by performing a foregoing, fast simulation with the one-dimensional model. With our choice of boundary conditions at the interfaces, reflections at the sub-domain boundaries can be avoided and the flow variables show a smooth transition at the interfaces. We numerically studied the role of the bed friction angle in both models (N-DAM and DAM). The compatibility of the Coulomb friction laws used in the respective models has been confirmed. We illustrated with examples that the inaccuracy of the coupled simulation increases substantially if the interface positions are not appropriately chosen. However, there is no strict rule for fixing the interface position and it is always a compromise between accuracy of the solution and computational cost. The performance of the coupling is very high. The numerical results obtained by the coupled model only deviate by few percentages from the ones generated with the full two-dimensional model. This

marginal error strongly justifies the coupling of the two-dimensional Coulomb-viscoplastic model with the one-dimensional model, based on the Mohr–Coulomb yield criterion. Remarkably, the run-time of the simulation can be reduced from days (for N-DAM) to hours (for coupled model) for the configurations considered here. We expect that in most applications the coupled model provides a significant improvement with respect to the computational effort, which will be even huge for large scale geophysical flows. In summary, we provide with the coupled model an attractive alternative to an expensive, full two-dimensional model.

Acknowledgements

We thank the German Research Foundation (DFG) for the financial support through contract no. PU 381-1,2: Transition of a granular flow into the deposit. We also sincerely thank the anonymous referees, and the editor, Michael D. Graham, for their constructive reviews and valuable suggestions that substantially helped to increase the clarity and quality of the paper.

References

[1] C. Ancey, Plasticity and geophysical flows: a review, J. Non-Newtonian Fluid Mech. 142 (1–3) (2007) 4–35.
[2] S.P. Pudasaini, K. Hutter, Avalanche Dynamics: Dynamics of Rapid Flows of Dense Granular Avalanches, Springer, Berlin, New York, 2007.
[3] Y. Forterre, O. Pouliquen, Flows of dense granular media, Annu. Rev. Fluid Mech. 40 (2008) 1–24.
[4] S.P. Pudasaini, S.A. Miller, The hypermobility of huge landslides and avalanches, Eng. Geol. 157 (2013) 124–132.
[5] S.P. Pudasaini, K. Hutter, S.S. Hsiau, S.C. Tai, Y. Wang, R. Katzenbach, Rapid flow of dry granular materials down inclined chutes impinging on rigid walls, Phys. Fluids 19 (2007) 053302.
[6] S.P. Pudasaini, C. Kröner, Shock waves in rapid flows of dense granular materials: theoretical predictions and experimental results, Phys. Rev. E 78 (4) (2008) 041308.
[7] P. Jop, Y. Forterre, O. Pouliquen, A constitutive law for dense granular flows, Nature 441 (7094) (2006) 727–730.
[8] N.J. Balmforth, I. Frigaard, Viscoplastic fluids: from theory to application, J. Non-Newtonian Fluid Mech. 142 (1–3) (2007) 1–3.
[9] S. Moriguchi, R.I. Borja, A. Yashima, K. Sawada, Estimating the impact force generated by granular flow on a rigid obstruction, Acta Geotech. 4 (1) (2009) 57–71.
[10] Eugene Cook Bingham, Fluidity and Plasticity, McGraw-Hill, New York, 1922.
[11] J.D. Dent, T.E. Lang, Experiments on mechanics of flowing snow, Cold Reg. Sci. Technol. 5 (3) (1982) 253–258.
[12] B. Voight, J. Sousa, Lessons from ontake-san: a comparative analysis of debris avalanche dynamics, Eng. Geol. 38 (3G4) (1994) 261–297.
[13] K.X. Whipple, Open-channel flow of bingham fluids: applications in debris-flow research, J. Geol. (1997) 243–262.
[14] P. Gauer, A. Elverhoi, D. Issler, F.V. De Blasio, On numerical simulations of subaqueous slides: back-calculations of laboratory experiments of clay-rich slides, Norw. J. Geol. 86 (3) (2006) 295.
[15] B. Domnik, Shiva P. Pudasaini, Full two-dimensional rapid chute flows of simple viscoplastic granular materials with a pressure-dependent dynamic slip-velocity and their numerical simulations, J. Non-Newtonian Fluid Mech. 173 (2012) 72–86.
[16] S. Moriguchi, A. Yashima, K. Sawada, R. Uzuoka, M. Ito, Numerical simulation of flow failure of geomaterials based on fluid dynamics, Soils Found. 45 (2) (2005) 155–165.
[17] M. Massoudi, T.X. Phuoc, The effect of slip boundary condition on the flow of granular materials: a continuum approach, Int. J. Nonlinear Mech. 35 (4) (2000) 745–761.
[18] S.P. Pudasaini, Y. Wang, K. Hutter, Velocity measurements in dry granular avalanches using particle image velocimetry technique and comparison with theoretical predictions, Phys. Fluids 17 (2005) 093301.
[19] K. Platzer, P. Bartelt, C. Jaedicke, Basal shear and normal stresses of dry and wet snow avalanches after a slope deviation, Cold Reg. Sci. Technol. 49 (1) (2007) 11–25.
[20] K. Platzer, P. Bartelt, M. Kern, Measurements of dense snow avalanche basal shear to normal stress ratios (s/n), Geophys. Res. Lett. 34 (7) (2007) L07501.
[21] S.B. Savage, K. Hutter, The motion of a finite mass of granular material down a rough incline, J. Fluid Mech. 199 (1989) 177–215.
[22] J.M.N.T. Gray, M. Wieland, K. Hutter, Gravity-driven free surface flow of granular avalanches over complex basal topography, Proc. Roy. Soc. A – Math. Phys. 455 (1985) (1999) 1841.
[23] Y.C. Tai, S. Noelle, J.M.N.T. Gray, K. Hutter, Shock-capturing and front-tracking methods for granular avalanches, J. Comput. Phys. 175 (1) (2002) 269–301.
[24] S.P. Pudasaini, K. Hutter, Rapid shear flows of dry granular masses down curved and twisted channels, J. Fluid Mech. 495 (2003) 193–208.
[25] J.M.N.T. Gray, Y.-C. Tai, S. Noelle, Shock waves, dead zones and particle-free regions in rapid granular free-surface flows, J. Fluid Mech. 491 (2003) 161–181.
[26] K.M. Hákonardóttir, A.J. Hogg, Oblique shocks in rapid granular flows, Phys. Fluids 17 (2005) 077101.
[27] J.F. Boudet, Y. Amarouchene, B. Bonnier, H. Kellay, The granular jump, J. Fluid Mech. 572 (2007) 413–432.
[28] X. Cui, J.M.N.T. Gray, T. Jóhannesson, Deflecting dams and the formation of oblique shocks in snow avalanches at flateyri, Iceland, J. Geophys. Res. 112 (F4) (2007) F04012.
[29] J.M.N.T. Gray, X. Cui, Weak, strong and detached oblique shocks in gravity-driven granular free-surface flows, J. Fluid Mech. 579 (2007) 113.
[30] B. Akers, O. Bokhove, Hydraulic flow through a channel contraction: multiple steady states, Phys. Fluids 20 (056601) (2008) 056601.
[31] C.G. Johnson, J.M.N.T. Gray, Granular jets and hydraulic jumps on an inclined plane, J. Fluid Mech. 675 (1) (2011) 87–116.
[32] X. Cui, J.M.N.T. Gray, Gravity-driven granular free-surface flow around a circular cylinder, J. Fluid Mech. 720 (2013) 314–337.
[33] K. Hutter, Y. Wang, S.P. Pudasaini, The Savage–Hutter avalanche model: how far can it be pushed?, Philos T. Roy. Soc. A 363 (1832) (2005) 1507–1528.
[34] S.P. Pudasaini, Y. Wang, K. Hutter, Modelling debris flows down general channels, Nat. Hazard Earth Syst. 5 (6) (2005) 799–819.
[35] S.P. Pudasaini, Y. Wang, K. Hutter, Rapid motions of free-surface avalanches down curved and twisted channels and their numerical simulation, Philos. T. Roy. Soc. A 363 (1832) (2005) 1551.
[36] S.P. Pudasaini, Y. Wang, L.T. Sheng, K. Hutter, R. Katzenbach, Avalanching granular flows down curved and twisted channels: theoretical and experimental results, Phys. Fluids 20 (2008) 073302.
[37] S.P. Pudasaini, B. Domnik, Energy considerations in accelerating rapid shear granular flows, Nonlinear Proc. Geophys. 16 (3) (2009) 399–407.
[38] L. Formaggia, J.F. Gerbeau, F. Nobile, A. Quarteroni, On the coupling of 3d and 1d Navier–Stokes equations for flow problems in compliant vessels, Comput. Method Appl. Mech. Eng. 191 (6) (2001) 561–582.
[39] E. Miglio, S. Perotto, F. Saleri, A multiphysics strategy for free surface flows, in: R. Kornhuber, R.W. Hoppe, J. Periaux, O. Pironneau, O. Widlund, J. Xu (Eds.), Domain Decomposition Methods in Science and Engineering, Springer, 2004, pp. 395–402.
[40] GDR MiDi, On dense granular flows, Eur. Phys. J. E 14 (2004) 341–365.
[41] F. da Cruz, S. Emam, M. Prochnow, J.-N. Roux, F. Chevoir, Rheophysics of dense granular materials: discrete simulation of plane shear flows, Phys. Rev. E 72 (2) (2005) 021309.
[42] H.P. Zhu, Z.Y. Zhou, R.Y. Yang, A.B. Yu, Discrete particle simulation of particulate systems: a review of major applications and findings, Chem. Eng. Sci. 63 (23) (2008) 5728–5770.
[43] Ivan Iordanoff, M.M. Khonsari, Granular lubrication: toward an understanding of the transition between kinetic and quasi-fluid regime, J. Tribol. 126 (1) (2004) 137–145.
[44] T.C. Papanastasiou, Flows of materials with yield, J. Rheol. 31 (1987) 385.
[45] W. Prager, D.C. Drucker, Soil mechanics and plastic analysis or limit design, Q. Appl. Math. 10 (2) (1952) 157–165.
[46] K. Oda, S. Moriguchi, I. Kamiishi, A. Yashima, K. Sawada, A. Sato, Simulation of a snow avalanche model test using computational fluid dynamics, Ann. Glaciol. 52 (58) (2011) 57.
[47] P.M. Gresho, R.L. Sani, On pressure boundary conditions for the incompressible Navier–Stokes equations, Int. J. Numer. Meth. Fl. 7 (10) (1987) 1111–1145.
[48] R.L. Sani, J. Shen, O. Pironneau, P.M. Gresho, Pressure boundary condition for the time-dependent incompressible Navier–Stokes equations, Int. J. Numer. Meth. Fl. 50 (6) (2006) 673–682.
[49] M. Griebel, T. Dornseifer, T. Neunhoeffer, Numerical Simulation in Fluid Dynamics: A Practical Introduction, Society for Industrial and Applied Mathematics, Philadelphia, 1997.
[50] F.H. Harlow, J.E. Welch, Numerical calculation of time-dependent viscous incompressible flow of fluid with free surface, Phys. Fluids 8 (12) (1965) 2182–2189.
[51] M.F. Tomé, J.L. Doricio, A. Castelo, J.A. Cuminato, S. McKee, Solving viscoelastic free surface flows of a second-order fluid using a marker-and-cell approach, Int. J. Numer. Meth. Fl. 53 (4) (2007) 599–627.
[52] E. Muravleva, Finite-difference schemes for the computation of viscoplastic medium flows in a channel, Math. Models Comput. Simul. 1 (2009) 768–779.
[53] M.J.D. Powell, A hybrid method for nonlinear equations, Numer. Meth. Nonlinear Alg. Equ. 6 (1970) 87–114.
[54] M. Galassi et al., GNU Scientific Library: Reference Manual. Network Theory, 2009. ISBN 0954612078.
[55] Y.C. Tai, J.M.N.T. Gray, Limiting stress states in granular avalanches, Ann. Glaciol. 26 (1998) 272–276.
[56] M. Mergili, K. Schratz, A. Ostermann, W. Fellin, Physically-based modelling of granular flows with open source gis, Nat. Hazard Earth Syst. 12 (1) (2012) 187–200.
[57] S.P. Pudasaini, A general two-phase debris flow model, J. Geophys. Res. 117 (2012) F03010.
[58] R.M. Beam, R.F. Warming, An implicit finite-difference algorithm for hyperbolic systems in conservation-law form, J. Comput. Phys. 22 (1) (1976) 87–110.